A Journal of the Gesellschaft Deutscher Chemiker

Angewandte International Edition GDCh Chemie

www.angewandte.org

Accepted Article

Title: Reviving Cost-Effective Organic Cathodes in Halide-Based All-Solid-State Lithium Batteries

Authors: Yingjie Gao, Jiamin Fu, Yang Hu, Feipeng Zhao, Weihan Li, Sixu Deng, Yipeng Sun, Xiaoge Hao, Jinjin Ma, Xiaoting Lin, Changhong Wang, Ruying Li, and Xueliang Sun

To be cited as: *Angew. Chem. Int. Ed.* **2024**, e202403331

Link to VoR: https://doi.org/10.1002/anie.202403331

WILEY VCH

10.1002/anie.202403331

WILEY VCH

COMMUNICATION

Reviving Cost-Effective Organic Cathodes in Halide-Based All-Solid-State Lithium Batteries

Yingjie Gao,[a] Jiamin Fu,[a] Yang Hu,[a] Feipeng Zhao,[a] Weihan Li,[a] Sixu Deng,[a] Yipeng Sun,[a] Xiaoge Hao,[a] Jinjin Ma,[a] Xiaoting Lin,[a] Changhong Wang,[b] Ruying Li,[a] and Xueliang Sun*[a][b]

[a] Y. Gao, Dr. J. Fu, Y. Hu, Dr. F. Zhao, Dr. W. Li, Dr. S. Deng, Dr. Y. Sun, X. Hao, J. Ma, Dr. X. Lin, R. Li, Prof. X. Sun
Department of Mechanical and Materials Engineering
University of Western Ontario
1151 Richmond St, London, Ontario, N6A 3K7 (Canada)
E-mail: xsun9@uwo.ca

[b] Prof. C. Wang, Prof. X. Sun
Eastern Institute for Advanced Study, Eastern Institute of Technology
Ningbo, Zhejiang 315200 (P.R. China)

Supporting information for this article is given via a link at the end of the document.

Abstract: The evolution of inorganic solid electrolytes has revolutionized the field of sustainable organic cathode materials, particularly by addressing the dissolution problems in traditional liquid electrolytes. However, current sulfide-based all-solid-state lithium-organic batteries still face challenges such as high working temperatures, high costs, and low voltages. Here, we design an all-solid-state lithium battery based on a cost-effective organic cathode material phenanthrenequinone (PQ) and a halide solid electrolyte Li_2ZrCl_6. Thanks to the good compatibility between PQ and Li_2ZrCl_6, the PQ cathode achieved a high specific capacity of 248 mAh g^{-1} (96% of the theoretical capacity), a high average discharge voltage of 2.74 V (vs. Li^+/Li), and a good capacity retention of 95% after 100 cycles at room temperature (25 °C). Furthermore, the interactions between the high-voltage carbonyl PQ cathode and both sulfide and halide solid electrolytes, as well as the redox mechanism of the PQ cathode in all-solid-state batteries, were carefully studied by a variety of advanced characterizations. We believe such a design and the corresponding investigations into the underlying chemistry give insights for the further development of practical all-solid-state lithium-organic batteries.

As electric vehicles and smart power grids rapidly expand, the traditional transition metal oxide cathode materials used in current lithium-ion batteries (LIBs) are increasingly challenged by high costs, low resource abundance, and limited capacity.[1, 2] Metal-free organic cathode materials have emerged as a promising alternative, offering sustainability, flexibility, and competitive energy densities.[3-5] Unfortunately, most organic small molecules suffer from dissolution in conventional liquid organic electrolytes, resulting in shuttle issues and rapid capacity loss.[6-8] To overcome these obstacles, substantial efforts have been made on regulating the structures of organic materials,[9] including polymerization,[10] salt formation,[11] and specific molecular structure designs.[12] However, these approaches often require additional synthetic steps and introduce non-electrochemically active groups (e.g., polymer backbones), which increase costs while reducing specific capacity. Therefore, researchers continue to explore more effective and efficient methods.

In recent years, the rapid development of all-solid-state lithium batteries (ASSLBs) has opened new avenues for this field. ASSLBs are regarded as one of the most promising next-generation battery technologies because of their use of non-flammable solid electrolytes (SEs). This configuration not only enhances safety but also allows for the potential use of lithium metal as an anode, offers a wide operating temperature range, and reduces packaging requirements.[13-15] More importantly, the inherent properties of inorganic SEs could intrinsically address the dissolution and shuttle issues associated with organic cathode materials, paving the way for utilizing readily available and cost-effective commercial organic small molecules as cathode materials.[16, 17]

To date, a diverse range of inorganic SEs with distinct characteristics have been developed, such as oxides, sulfides, and halides.[14, 18, 19] Among them, sulfide-based SEs (e.g., $Li_{10}GeP_2S_{12}$ and Li_6PS_5Cl) have garnered significant attention because of their high ionic conductivity and good processibility.[20] However, they still face problems including narrow electrochemical windows,[14, 21] incompatibility with high-voltage cathode materials,[14, 22] and moisture sensitivity.[14, 23] On the other hand, a series of halide-based SEs (e.g., Li_3YCl_6, Li_3InCl_6, and Li_2ZrCl_6) were recently reported, exhibiting similarly high ionic conductivity and ease of processing.[24] Additionally, halide-based SEs generally possess remarkably improved compatibility with coating-free cathode materials compared to sulfide-based SEs, due to the superior high-voltage stability of chlorine anions.[25-27]

Given the unique advantages of SEs for organic cathode materials, a number of them, including pyrene-4,5,9,10-tetraone (PTO),[28] poly(anthraquinonyl sulfide) (PAQS),[29] 5,7,12,14-pentacenetetrone (PT),[30] polyimide (PI),[31] tetralithium salts of 2,5-dihydroxyterephthalic acid (Li_4DHTPA),[32] and the complex of Li_4DHTPA and Tetracyanoquinodimethane ($Li_4DHTPA{\cdot}2TCNQ$)[33] have been studied in ASSLBs based on several typical sulfide SEs (e.g., Li_3PS_4, Li_6PS_5Cl, and $Li_7P_3S_{11}$) in the past two years. As expected, the all-solid-state configuration eliminated the high solubility issue of organic cathode materials in electrolytes, and some achieved impressive performance like high capacity and decent cycling stability. Nonetheless, several issues remain that need to be understood and resolved: 1) high working temperatures: all the reported

10.1002/anie.202403331

sulfide-based all-solid-state lithium-organic batteries need to work at an elevated temperature (e.g., 60 °C), despite the high ionic conductivity of sulfide SEs (e.g., > 10^{-3} S cm^{-1} of Li_6PS_5Cl at 25 °C); 2) low operating voltages: all the reported organic cathode materials showed relatively low operating voltages of 1.9 – 2.4 V vs. Li^+/Li with sulfide SEs, which were commonly lower than their counterparts in liquid electrolytes; 3) expensive synthetic route: most of the current high-performance organic cathode materials were actually synthesized through specialized and expensive routes, although they were claimed to have potentially low costs. To promote the practical application of organic cathode materials, it is still necessary to design a room-temperature, high-voltage, and cost-effective all-solid-state lithium-organic battery, as well as gain deeper insights into the mechanisms.

Here, we scrutinized the existing family of organic cathode materials and selected phenanthrenequinone (PQ) as an example for our research due to its easy synthesis, low cost, high capacity, and high voltage. We initially investigated the compatibilities between PQ cathodes and both sulfide and halide SEs by a series of state-of-the-art characterizations, such as various synchrotron-based X-ray technologies. Both chemical and electrochemical incompatibilities of the PQ cathode and sulfide SE Li_6PS_5Cl (LPSC) were revealed, which were mainly ascribed to side reactions between them. By contrast, PQ cathodes still demonstrated a high capacity for the reversible de/intercalation of lithium after they were thoroughly mixed with the Li_2ZrCl_6 (LZC) SE. The conjugated carbonyl groups (C=O), serving as redox centers in PQ, maintained favorable electrochemical activity within the LZC SE, and their reversible evolution during the discharge and charge process was also clearly disclosed. Based on the results, we designed an all-solid-state lithium-organic battery using the commercial and ultracheap organic small molecule PQ as the cathode and the cost-effective metal halide LZC as the SE. The PQ cathode with LZC SE achieved outstanding performance including a high specific capacity of 248 mAh g^{-1} (96% of the theoretical capacity), a high average discharge voltage of 2.74 V (vs. Li^+/Li), and an excellent capacity retention of 95% after 100 cycles at room temperature (25 °C), which is superior to that of previous reports in this area. The successful application of organic carbonyl cathode materials in halide-based ASSLBs, and the systematic and detailed study of the compatibility between them and SEs could contribute to both organic electrode and solid-state battery research communities.

PQ can be easily synthesized by a one-step reaction using chromic acid and phenanthrene,[34] both of which are low-cost and widely used industrial chemicals. PQ itself is also commercially available, so we used purchased PQ directly in this study. The commercial PQ was orange powder (Figure S1), and its microscopic morphology was revealed by synchrotron-based

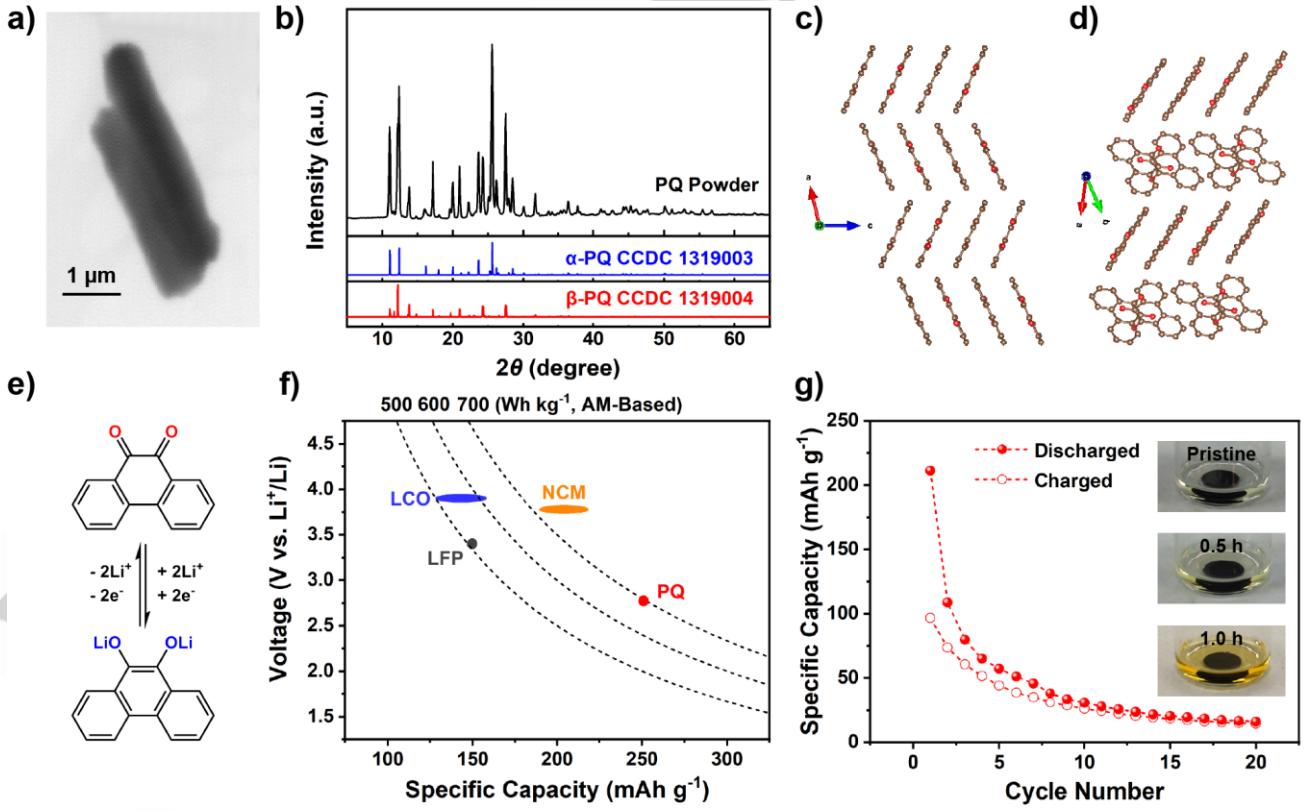

Figure 1. (a) STXM image of PQ; (b) SXRD pattern of PQ powder and the simulated XRD patterns of α-PQ (CCDC 1319003) and β-PQ (CCDC 1319004); Crystal structures of α-PQ (c) and β-PQ (d). The red and brown balls represent O and C atoms, respectively. The H atoms are omitted. The visualization was carried out by VESTA;[36] (e) Electrochemical redox mechanism of PQ; (f) Comparison of energy density between PQ and representative inorganic oxide cathode materials based on the mass of active materials (AM); (g) Cycle performance of PQ cathode in liquid electrolyte 1 M $LiPF_6$/EC+DEC+DMC. The insertions are the photos of a PQ cathode film soaked in the liquid electrolyte after different times.

10.1002/anie.202403331

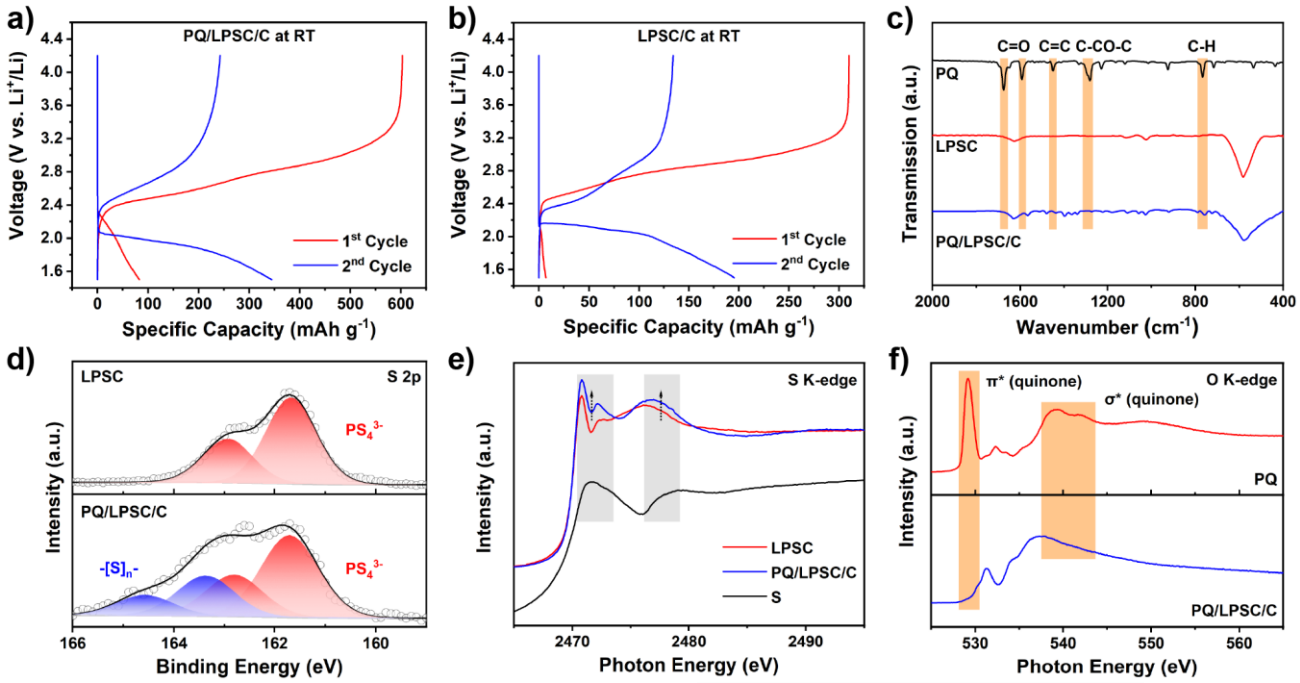

Figure 2. (a) Voltage curves of PQ/LPSC/C cathode at 0.1 C in the initial two cycles at room temperature; (b) Voltage curves of LPSC/C cathode at 0.1 C in the initial two cycles at room temperature; (c) FTIR spectra of PQ, LPSC, and PQ/LPSC/C; (d) S 2p XPS spectra of LPSC and PQ/LPSC/C; (e) S *K*-edge XANES spectra of LPSC, PQ/LPSC/C, and S; (f) O *K*-edge XANES spectra of PQ and PQ/LPSC/C.

scanning transmission X-ray microscopy (STXM) and scanning electron microscopy (SEM) to be rod-like microparticles (Figure 1a and S2).[35] Interestingly, the synchrotron X-ray diffraction (SXRD) patterns indicated that the commercial PQ was a mixture of two phases: α-PQ and β-PQ (Figure 1b). The PQ molecules in α-PQ were parallel to each other in columns along the c axis, while molecules in β-PQ were paired by approaching their carbonyl groups to each other (Figure 1c, 1d, and S3).

PQ has a typical n-type quinone structure with conjugated carbonyl groups, which can be electrochemically reduced and oxidized based on a reversible enolization-like process (Figure 1e). The two-electron redox reaction and the small molecular mass of PQ lead to a high capacity, and the ortho-quinone structure allows PQ to have a relatively high voltage compared to para-quinones, such as its isomer anthraquinone (AQ).[6-9, 37] Therefore, PQ cathodes have a competitive energy density of ~ 700 Wh kg^{-1}, which is beyond those of traditional $LiCoO_2$ (LCO) and $LiFePO_4$ (LFP) and is close to that of advanced ternary cathode materials (NCM) (Figure 1f). However, its application as a cathode material for LIBs has been plagued by solubility issues like other small molecules for a long time.[38] As shown in Figure 1g, the capacity of the PQ cathode in liquid electrolyte 1 M $LiPF_6$/EC+DEC+DMC (EC: Ethylene Carbonate, DEC: Diethyl Carbonate, DMC: Dimethyl Carbonate) decayed rapidly to nearly zero in 20 cycles. It was clear that the liquid electrolyte turned to orange after placing a PQ cathode film in it for 1 h, suggesting the fast dissolution of PQ in the electrolyte.

Unlike organic liquid electrolytes, inorganic SEs are believed to fundamentally inhibit the loss of organic cathode materials.[16, 17] Given that some sulfide-based all-solid-state lithium-organic batteries have been reported, we first tried the PQ cathode with a representative sulfide SE Li_6PS_5Cl (LPSC). The LPSC, synthesized by ball milling and post annealing, showed a cubic structure with $F\bar{4}3m$ space group and a high ionic conductivity of 1.5×10^{-3} S cm^{-1}, which were consistent with previous reports (Figure S4).[39] In order to ensure sufficient ionic and electronic conductivity in the cathode, PQ, LPSC, and conductive carbon (C) were thoroughly mixed using low-speed ball milling. The cathode delivered a moderate capacity of 83 mAh g^{-1} at 0.1 C (1 C = 257 mA g^{-1}) in the first discharge, but the corresponding average voltage was only 1.92 V vs. Li^+/Li (Figure 2a). The voltage was distinctly lower than that of PQ's standard redox reaction (> 2.5 V vs. Li^+/Li), implying the activity of PQ cathodes had been seriously damaged in LPSC. The following charge process did not accord with the electrochemical behavior of PQ neither, exhibiting an abnormal capacity of approximately 600 mAh g^{-1}. Although relatively reversible discharged and charged voltage curves were achieved in the second cycle, their polarization was about 0.9 V, and the voltage plateau was actually very similar to that of S/S^{2-}.[21] The To understand this phenomenon, we prepared a LPSC/C composite in the same way. Its electrochemical behavior was fairly close to that of PQ/LPSC/C, demonstrating the observed discharge and charge activity in PQ/LPSC/C was mainly contributed by the decomposition of LPSC and the subsequent redox reactions (Figure 2b). The only obvious difference was the initial discharged capacity of PQ/LPSC/C, which was possibly from the reaction products of PQ and LPSC. The cyclic voltammetry (CV) curves of PQ/LPSC/C

10.1002/anie.202403331

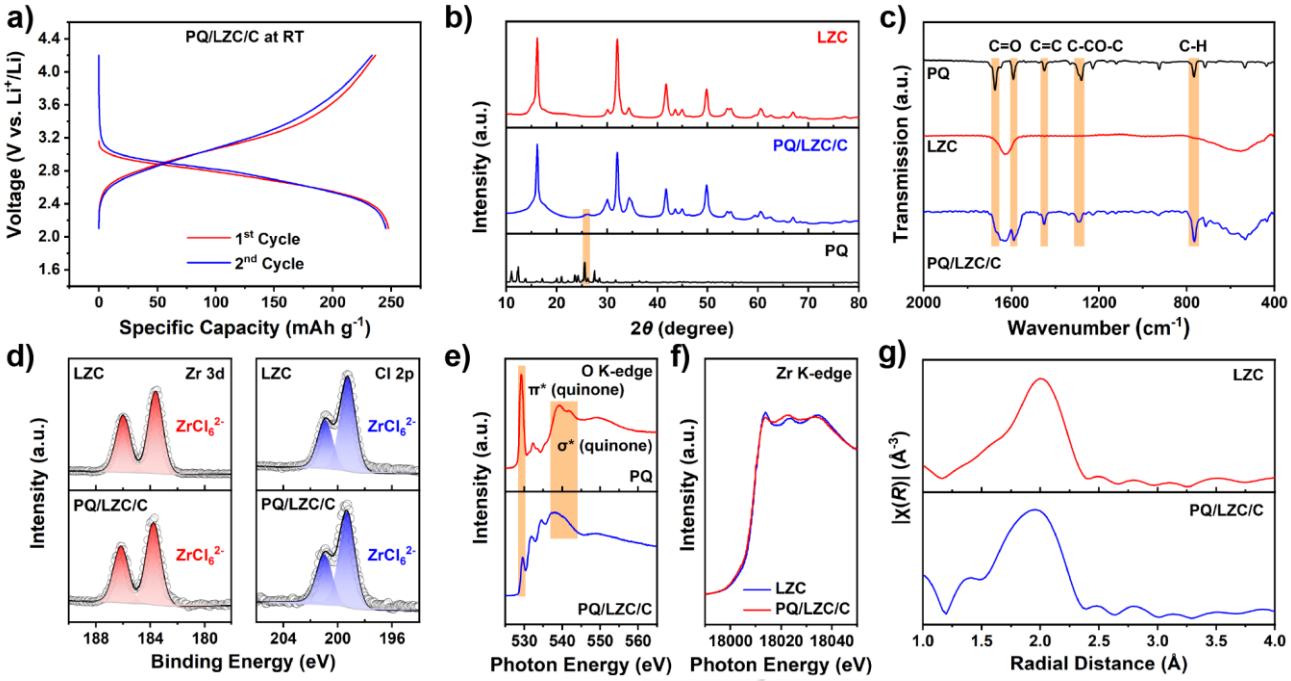

Figure 3. (a) Voltage curves of PQ/LZC/C cathode at 0.1 C in the initial two cycles at room temperature; (b) SXRD patterns of PQ, LZC, and PQ/LZC/C powder; (c) FTIR spectra of PQ, LZC, and PQ/LZC/C; (d) Zr 3d and Cl 2p XPS spectra of LZC and PQ/LZC/C; (e) O *K*-edge XANES spectra of PQ and PQ/LZC/C; (f) Zr *K*-edge XANES spectra of LZC and PQ/LZC/C; (g) k^2-weighted EXAFS spectra in *R* space of LZC and PQ/LZC/C.

and LPSC/C also illustrated that the electrochemical window of LPSC was too narrow to match the high-voltage PQ cathode, and that PQ was unable to display its lithium storage activity in LPSC (Figure S5).

For further investigation into the reactions between PQ and LPSC, a range of characterizations focusing on chemical properties were employed. In the Fourier transform infrared spectroscopy (FTIR) analysis of PQ, characteristic peaks associated with C=O groups were observed at 1676 and 1595 cm^{-1} (Figure 2c). Concurrently, peaks attributable to C=C, C-CO-C, and C-H groups were evident at 1452, 1284, and 766 cm^{-1}, respectively, aligning well with the ortho-quinone structure.[40] The LPSC SE also exhibited several characteristic peaks in its FTIR spectrum, with the strongest, a broad peak, appearing near 582 cm^{-1}.[41] These peaks of LPSC were retained in the spectrum of the PQ/LPSC/C composite, yet all of the aforementioned characteristic peaks of PQ disappeared. Additionally, many unknown small peaks emerged in the spectrum of PQ/LPSC/C, indicating that all PQ had undergone chemical reactions with LPSC during the mixing process, resulting in the formation of new products. The oxidation of S^{2-} in LPSC was further revealed by the X-ray photoelectron spectroscopy (XPS) analysis of S 2p (Figure 2d). Compared to the spectrum of pristine LPSC, a pair of peaks located at 163.4 and 164.6 eV, respectively, appeared in that of PQ/LPSC/C, which were attributed to the formation of -$[S]_n$-.[28] The X-ray absorption near edge structure (XANES) analysis on S *K*-edge also uncovered the valence evolution of S (Figure 2e).[42] The XANES spectrum of PQ/LPSC/C noticeably intensified near 2472 and 2478 eV, agreeing well with the features of sulfur power, which was in a higher oxidation state. Correspondingly, the sharp and intensive peak at 529.2 eV and the broad peak at 539.3 eV in the O *K*-edge XANES spectrum of PQ, attributed to the 1s - π* resonances and the 1s - σ* transition of O in C=O bonds, respectively, disappeared in that of PQ/LPSC/C (Figure 2f).[43] At the same time, a new feature at about 531.2 eV appeared, which could be ascribed to the formation of C-O bonds. Besides, the O 1s XPS peak of PQ shifted to a higher binding energy in the spectrum of PQ/LPSC/C, also demonstrating the reduction of C=O groups (Figure S6).[12, 40]

In conclusion, we identified two primary reasons for the incompatibility between the sulfide SE LPSC and the organic cathode material PQ: Firstly, the narrow electrochemical window of LPSC limited its compatibility, as the redox potential of PQ cathodes exceeded LPSC's antioxidation potential. Secondly, significant interfacial reactions between PQ and LPSC occurred during the mixing process. The carbonyl (C=O) groups in PQ were readily reduced by the S^{2-} in LPSC, leading to the loss of their redox activity.

Given that halide SEs have demonstrated superior cathode compatibility to sulfide SEs in numerous reports, we further explored the application of PQ cathodes within halide SEs. Herein, we synthesized a cost-effective Li_2ZrCl_6 (LZC) SE using a ball-milling method. The LZC SE exhibited an ionic conductivity of approximately 6×10^{-4} S cm^{-1} at room temperature and a low-crystallinity trigonal phase with a $P\bar{3}m1$ space group (Figure S7). Upon blending with LZC and C via the same method, PQ displayed a specific capacity of 248 mAh g^{-1} and a high voltage plateau of 2.74 V vs. Li^+/Li at 0.1 C at room temperature, both

10.1002/anie.202403331

approaching their theoretical values (Figure 3a). Concurrently, the coincidence of the first and second charge-discharge curves indicated the robust electrochemical activity of PQ within the LZC SE. The CV curve of PQ/LZC/C at 0.1 mV s^{-1} exhibited two pairs of broad redox peaks, aligning with the sloping plateaus during constant current charge-discharge (Figure S8). Furthermore, LZC/C demonstrated commendable stability within a voltage range of 2.1 - 4.2 V vs. Li^+/Li, implying that the observed capacity was predominantly contributed by the lithium deintercalation reaction of PQ (Figure S9).

SXRD patterns revealed that LZC retained its initial high ionic conductivity crystal structure after mixing with PQ and C (Figure 3b). Simultaneously, the strongest peak signal of PQ was faintly observable in the SXRD patterns of PQ/LZC/C. This reduced strength might stem from the ball-milling mixing process, in which the crystallinity of PQ could decrease. The uniform distribution of PQ without its characteristic rod-like shape in the LZC SE matrix was observed through SEM images, and was further verified by the corresponding energy dispersive spectroscopy (EDS) mapping of Zr, Cl, C, and O elements (Figure S10). The FTIR spectrum of LZC was simpler compared to LPSC, presenting only two broad peaks near 1630 and 555 cm^{-1}, respectively (Figure 3c). In contrast to the results with sulfide SEs, the characteristic peak signals of PQ in the PQ/LZC/C FTIR spectrum were retained without deviation, indicating that the molecular structure of PQ remained intact after thorough contact with LZC. LZC itself was also undamaged after mixing, which was substantiated by the lack of noticeable shift in the Zr 3d and Cl 2p XPS peaks (Figure 3d). Similarly, the XPS peaks from the O in PQ did not exhibit significant changes pre- and post-mixing (Figure S11). Further XAS analysis of the O element revealed no energy shift in its 1s-π* and 1s-σ* transitions in the characteristic quinone structure, corroborating the commendable electrochemical activity of PQ within LZC (Figure 3e). Intriguingly, in the O *K*-edge XANES spectrum of PQ/LZC/C, two new peaks emerged near 531.8 eV and 534.4 eV, implying there could be slight interactions between the O of PQ and LZC. For LZC and PQ/LZC/C, a tiny difference in the states of Zr were disclosed by carefully comparing their *K*-edge XANES spectra (Figure 3f). The three features located at 18013.8, 18023.6, and 18034.8 eV, respectively, could be attributed to the three shells around Zr atoms caused by the distortion of Zr-Cl bonds in the $[ZrCl_6]^{2-}$ octahedrons (Figure S12).[44] All of the three minute peaks at the whiteline and the first derivative peak were located at the same photon energy points after mixing, validating that the overall structure of LZC SE remained unchanged (Figure S13). Nonetheless, subtle changes in the relative intensities of the three characteristic peaks suggested minor adjustments in the local structure surrounding the Zr atoms. Moreover, the weak interaction between the O from PQ and the Zr from LZC was further identified by the extended X-ray absorption fine structure (EXAFS) spectra of Zr *K*-edge in *R* space (Figure 3g). The broad peak located at around 2 Å belonged to the Zr-Cl paths, while the shoulder peak that arose at a smaller distance could represent the formation of Zr-O paths (Figure S14). The wavelet transformation (WT) of EXAFS spectra also supported this conclusion (Figure S15).[45] This might also account for the distinct charge/discharge profiles and slightly elevated voltage plateaus exhibited by PQ in the LZC SE compared to its behavior in liquid electrolytes.[13, 46]

Overall, our study showed that PQ cathodes and LZC SEs demonstrated excellent compatibility. PQ was able to reversibly achieve a high capacity and a high voltage in the LZC SE. In-depth analyses revealed a weak interaction between the O atoms in the C=O groups of PQ and the Zr central atoms in LZC. Interestingly, this interaction did not detract from the electrochemical activity of PQ or the lithium-ion transport capability of LZC and even slightly enhanced the operating voltage of the PQ cathode.

Compared to previous all-solid-state lithium-organic batteries, this work based on the PQ cathode and the LZC SE displayed advantages in several aspects. Firstly, PQ, as a simple small molecule, showcased a distinct cost advantage. We summarized the synthetic routes of organic cathode materials previously reported for use in solid-state batteries and estimated their industrial raw material costs using a linear fitting method (Table S1-9).[24, 47, 48] Among them, the cost of PQ was estimated to be as low as approximately 19.9 \$ kg^{-1}. Even though some materials exhibit ultra-high specific capacity due to their unique molecular design (such as PTO), they were at a disadvantage in terms of the ratio of energy density to cost, i.e., specific cost. PQ demonstrated a specific cost of only 0.03 \$ Wh^{-1}, significantly lower than other organic cathode materials and also superior to the classical LCO cathode (Figure 4a). Secondly, previously reported all-solid-state lithium-organic batteries could only operate at elevated temperatures of 55-60 °C, even though sulfide SEs were famous for their high room-temperature ionic conductivity. In contrast, our work realized more practical room-temperature operating conditions (Figure 4b). Moreover, it is worth noting that while some organic cathode materials exhibited high discharge voltages in liquid electrolytes (e.g., ~2.6 V vs. Li^+/Li for PTO), their corresponding voltages in sulfide SEs were only about 2.1 V. This voltage mismatch and high-temperature operating condition suggested the incompatibility between organic cathode materials and sulfide SEs to some degree. On the contrary, the PQ cathode in LZC SE displayed a working voltage of 2.74 V vs. Li^+/Li, noticeably superior to other reports. At room temperature, the PQ cathode also exhibited acceptable rate performance (Figure 4c). When the current rate returned to a small value, its capacity almost fully recovered (Figure S16). At a moderate current density of 0.3 C, the capacity of the PQ cathode in LZC stabilized after a few initial activation cycles, maintaining an excellent capacity retention of 95% after 100 cycles (Figure 4d). The activation process could be ascribed to the optimization of the Li^+ diffusion pathways within the PQ particles, as well as the gradual enhancement of ionic and electronic contact between the PQ particles and the LZC SE.[49] For PQ/LPSC/C, although the initial decomposition of LPSC provided additional capacity, it decayed very rapidly.

Subsequently, we delved further into the solid-phase redox process during the charging and discharging of the PQ cathode in LZC SE. In the ex-situ O *K*-edge XANES spectra, we clearly observed the 1s-π* and 1s-σ* features of C=O groups correspondingly disappearing and emerging during the

10.1002/anie.202403331

discharge/charge process (Figure 4e). Simultaneously, the 1s-σ* feature of C-O groups was only detected in the discharged state, confirming that the lithium storage reaction was based on the conversion between C=O and C-O-Li. Besides, the FTIR peaks of C=O groups' stretching vibration vanished in the discharged state and then recovered in the charged state (Figure 4f). The stretching vibration peaks of C=C and C-CO-C bonds, and the deformation vibration peak of C-H bonds, originating from the benzene skeleton of PQ, as well as the characteristic peaks of LZC, remained unchanged in different states. All of the features

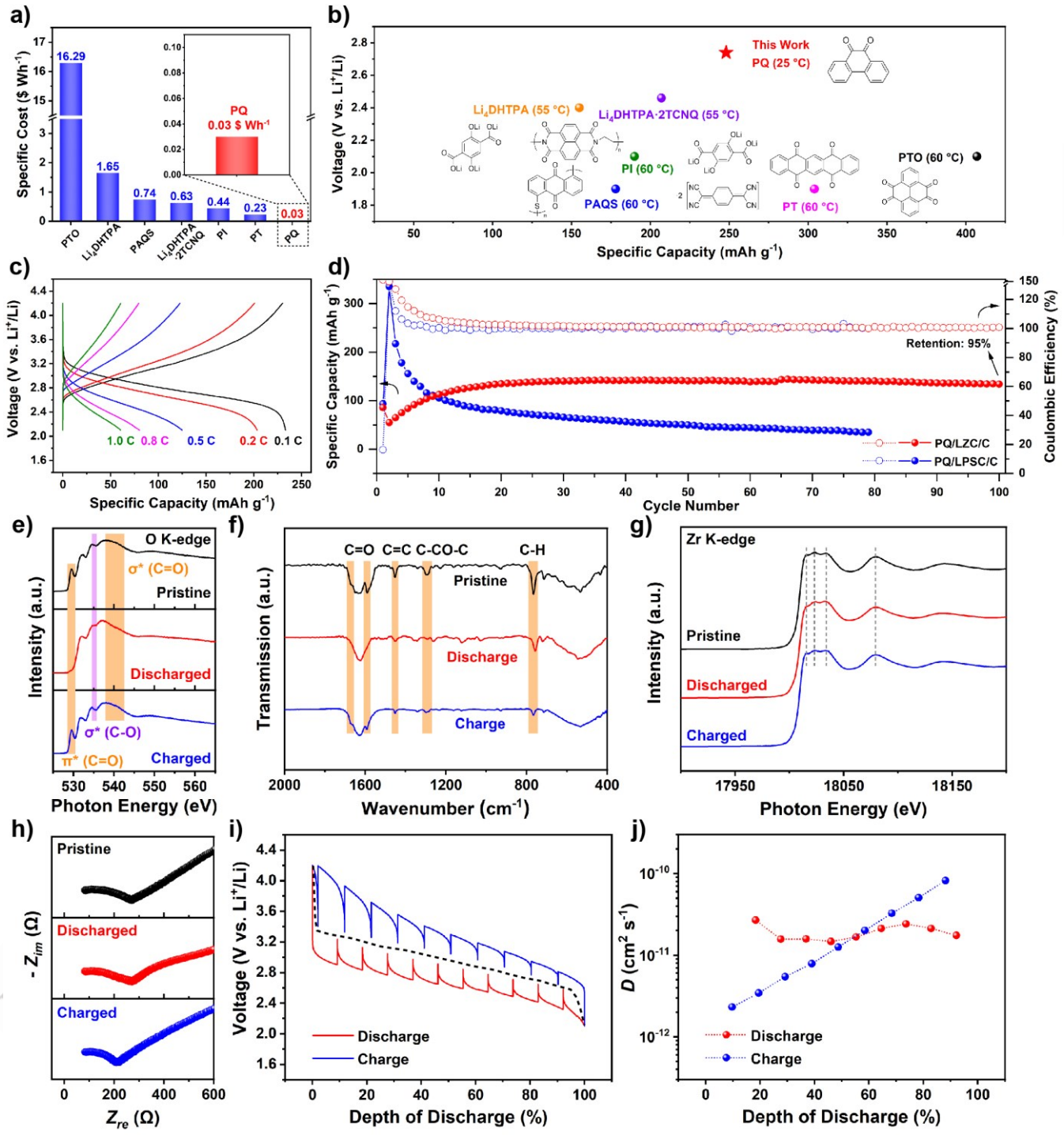

Figure 4. (a) Comparison of specific cost between PQ and previously reported organic cathode materials for all-solid-state lithium batteries; (b) Comparison of working voltage, specific capacity, and operating temperature between this work and previous reports regarding all-solid-state lithium-organic batteries; (c) Rate performance of PQ cathode in LZC SE at room temperature; (d) Cycle performance of PQ/LZC/C and PQ/LPSC/C with a current rate of 0.3 C at room temperature; (e) Ex-situ O *K*-edge XANES spectra, (f) Ex-situ FTIR spectra, and (g) Ex-situ Zr *K*-edge XANES spectra of PQ/LZC/C in pristine, discharged, and recharged states; (h) Nyquist plots of the all-solid-state Li-PQ battery in pristine, discharged, and recharged states; (i) GITT (red and blue) and QOCV (black) curves of PQ/LZC/C cathode at room temperature and the corresponding (j) diffusion coefficient *D* during the discharge and charge process.

in the Zr *K*-edge XANES spectra, under different states, also maintained a high degree of consistency, providing robust evidence for the stability of LZC throughout the electrochemical redox process (Figure 4g). The all-solid-state Li-PQ battery based on LZC demonstrated an overall impedance of approximately 210 - 260 Ω in the electrochemical impedance spectra (EIS) during the discharge and charge process, consistent with the stability exhibited by the LZC SE. (Figure 4h). For a deeper insight into the kinetic factors, the distribution of relaxation time (DRT) analysis was performed on the EIS data (Figure S17).[50] Four primary peaks were identified in the DRT spectra, located at 10^{-7}-10^{-6} s (P1), 10^{-2}-10^{-1} s (P2), 10^{-1}-10^{0} s (P3), and 10^{0}-10^{1} s (P4). They corresponded to physical contact, anode/SE interfaces, cathode/SE interfaces, and the Li^+ diffusion in cathodes, respectively.[51] The intensities of the cathode-related peaks P3 and P4 decreased as the battery was discharged, suggesting both of the PQ/LZC interface and the diffusion in PQ became more facile for the transportation of Li^+. After recharging, these kinetic processes slowed but showed optimization compared to the pristine state, suggesting that an activation process might occur inside the battery. The galvanostatic intermittent titration technique (GITT) was then employed to study the quasi-open-circuit voltage (QOCV) and the diffusion coefficient *D*. It was found that the GITT curves of discharge and charge basically coincided, confirming the reversibility of its redox reaction path (Figure 4i). The diffusion coefficient *D* remained essentially stable during the discharge process, but continuously diminished during charging, indicating that the extraction of Li^+ from PQ was more challenging than its insertion (Figure 4j). This provided a point of entry for future continuous improvements on the performance of all-solid-state Li-PQ batteries.

In summary, we scrutinized the compatibility of the organic cathode material PQ with different mainstream solid-state electrolytes. It was revealed that the side redox reactions between PQ and sulfide SEs and also the insufficient electrochemical stability of sulfide SEs, accounted for their incompatibility with PQ. By transforming the unstable S^{2-} anion framework into a Cl^- anion framework, we effectively improved the compatibility issue between the PQ cathode and SEs. In our design, the cost-effective and high-voltage PQ cathodes exhibited high performance at room temperature in halide-based all-solid-state batteries, attributable to the stability of LZC SE and the advantageous interaction between PQ and LZC. Furthermore, a detailed examination of the underlying chemistry governing the behaviors of the PQ cathode in SEs was conducted, furnishing guidelines for the development of practical all-solid-state lithium-organic batteries in future endeavors.

Acknowledgements

This research received support from the Natural Sciences and Engineering Research Council of Canada (NSERC), the Canada Research Chair Program (CRC), the Canada Foundation for Innovation (CFI), the Ontario Research Foundation (ORF), China Automotive Battery Research Institute Co., Ltd., Glabat Solid-State Battery Inc., and the University of Western Ontario (UWO). The synchrotron research was conducted at the SM, BXDS-WHE, SXRMB, SGM, and HXMA beamlines of the Canadian Light Source (CLS), a national research facility housed at the University of Saskatchewan, with support from the CFI, NSERC, National Research Council (NRC), Canadian Institutes of Health Research (CIHR), Government of Saskatchewan, and the University of Saskatchewan. Mr. Yingjie Gao and Dr. Weihan Li acknowledge the receipt of support from the CLSI Graduate and Post-Doctoral Student Travel Support Program. Dr. Weihan Li appreciates the funding support from Mitacs Accelerate Fellowships. The authors extend their heartfelt gratitude to Dr. Jian Wang, Dr. Graham King, Dr. Mohsen Shakouri, Dr. Zachary Arthur, and Dr. Ning Chen for their invaluable assistance at the CLS.

Keywords: organic cathodes • all-solid-state batteries • halide solid electrolytes • quinone • lithium batteries

[1]. D. Larcher, J.-M. Tarascon, *Nat. Chem.* **2015**, *7*, 19-29.
[2]. Y. S. Hu, *Nat. Energy* **2016**, *1*, 16042.
[3]. Y. Liang, Y. Yao, *Joule* **2018**, *2*, 1690-1706.
[4]. Y. Lu, J. Chen, *Nat. Rev. Chem.* **2020**, *4*, 127-142.
[5]. X. Chen, X. Yin, J. Aslam, W. Sun, Y. Wang, *Electrochem. Energy Rev.* **2022**, *5*, 12.
[6]. J. Kim, Y. Kim, J. Yoo, G. Kwon, Y. Ko, K. Kang, *Nat. Rev. Mater.* **2023**, *8*, 54-70.
[7]. P. Poizot, J. Gaubicher, S. Renault, L. Dubois, Y. Liang, Y. Yao, *Chem. Rev.* **2020**, *120*, 6490-6557.
[8]. Z. Song, H. Zhou, *Energy Environ. Sci.*, **2013**, *6*, 2280.
[9]. Z. Wu, Q. Liu, P. Yang, H. Chen, Q. Zhang, S. Li, Y. Tang, S. Zhang, *Electrochem. Energy Rev.* **2022**, *5*, 26.
[10]. a) Z. Song, H. Zhan, Y. Zhou, *Chem. Commun.* **2009**, 448-450; b) Z. Song, H. Zhan, Y. Zhou, *Angew. Chem. Int. Ed.* **2010**, *49*, 8444-8448; c) Z. Song, Y. Qian, M. L. Gordin, D. Tang, T. Xu, M. Otani, H. Zhan, H. Zhou, D. Wang, *Angew. Chem. Int. Ed.* **2015**, *54*, 13947-13951; d) Z. Song, Y. Qian, T. Zhang, M. Otani, H. Zhou, *Adv. Sci.* **2015**, 1500124.
[11]. a) S. Wang, L. Wang, K. Zhang, Z. Zhu, Z. Tao, J. Chen, *Nano Lett.* **2013**, *13*, 4404-4409; b) Z. Song, Y. Qian, X. Liu, T. Zhang, Y. Zhu, H. Yu, M. Otani, H. Zhou, *Energy Environ. Sci.* **2014**, *7*, 4077; c) J. Lee, M. J. Park, *Adv. Energy Mater.* **2017**, *7*, 1602279; d) T. Cai, Z. Hu, Y. Gao, G. Li, Z. Song, *Energy Storage Mater.* **2022**, *50*, 426-434.
[12]. a) Y. Liang, P. Zhang, J. Chen, *Chem. Sci.* **2013**, *4*, 1330; b) Y. Gao, G. Li, F. Wang, J. Chu, P. Yu, B. Wang, H. Zhan, Z. Song, *Energy Storage Mater.* **2021**, *40*, 31-40; c) Z. Chen, J. Wang, T. Cai, Z. Hu, J. Chu, F. Wang, X. Gan, Z, Song, *ACS Appl. Mater. Interfaces* **2022**, *14*, 27994-28003.
[13]. Z. Zhang, Y. Shao, B. Lotsch, Y.-S. Hu, H. Li, J. Janek, L. F. Nazar, C.-W. Nan, J. Maier, M. Armand, L. Chen, *Energy Environ. Sci.* **2018**, *11*, 1945.
[14]. R. Chen, Q. Li, X. Yu, L. Chen, H. Li, *Chem. Rev.* **2020**, *120*, 6820-6877.
[15]. T. Famprikis, P. Canepa, J. A. Dawson, M. S. Islam, C. Masquelier, *Nat. Mater.* **2019**, *18*, 1278-1291.
[16]. L. Zhao, A. E. Lakraychi, Z. Chen, Y. Liang, Y. Yao, *ACS Energy Lett.* **2021**, *6*, 3287-3306.
[17]. X. Gan, Z. Yang, Z. Song, *Batteries Supercaps* **2023**, *6*, e202300001.
[18]. W. Zhao, J. Yi, P. He, H. Zhou, *Electrochem. Energy Rev.* **2019**, *2*, 574-605.

[19]. Q. Liu, Q. Chen, Y. Tang, H.‐M. Cheng, *Electrochem. Energy Rev.* **2023**, *6*, 15.

[20]. a) F. Mizuno, A. Hayashi, K. Tadanaga, M. Tatsumisago, *Adv. Mater.* **2005**, 17, 7; b) H.-J. Deiseroth, S.-T. Kong, H. Eckert, J. Vannahme, C. Reiner, T. Zaiß, M. Schlosser, *Angew. Chem. Int. Ed.* **2008**, 47, 755-758; c) N. Kamaya, K. Homma, Y. Yamakawa, M. Hirayama, R. Kanno, M. Yonemura, T. Kamiyama, Y. Kato, S. Hama, K. Kawamoto, A. Mitsui, *Nat. Mater.* **2011**, *10*, 682-686; d) Y. Kato, S. Hori, T. Saito, K. Suzuki, M. Hirayama, A. Mitsui, M. Yonemura, H. Iba, R. Kanno, *Nat. Energy* **2016**, *1*, 16030; e) Y. Li, S. Song, H. Kim, K. Nomoto, H. Kim, X. Sun, S. Hori, K. Suzuki, N. Matsui, M. Hirayama, T. Mizoguchi, T. Saito, T. Kamiyama, R. Kanno, *Science* **2023**, *381*, 50-53.

[21]. a) F. Han, Y. Zhu, X. He, Y. Mo, C. Wang, *Adv. Energy Mater.* **2016**, *6*, 1501590; b) T. K. Schwietert, V. A. Arszelewska, C. Wang, C. Yu, A. Vasileiadis, N. J. J. de Klerk, J. Hageman, T. Hupfer, I. Kerkamm, Y. Xu, E. van der Maas, E. M. Kelder, S. Ganapathy, M. Wagemaker, *Nat. Mater.* **2020**, *19*, 428-435.

[22]. a) J. Auvergniot, A. Cassel, J.-B. Ledeuil, V. Viallet, V. Seznec, R. Dedryvère, *Chem. Mater.* **2017**, *29*, 3883-3890; b) X. Li, Z. Ren, M. N. Banis, S. Deng, Y. Zhao, Q. Sun, C. Wang, X. Yang, W. Li, J. Liang, X. Li, Y. Sun, K. Adair, R. Li, Y. Hu, T.-K. Sham, H. Huang, L. Zhang, S. Lu, J. Luo, X. Sun, *ACS Energy Lett.* **2019**, *4*, 2480-2488.

[23]. P. Lu, D. Wu, L. Chen, H. Li, F. Wu, *Electrochem. Energy Rev.* **2022**, *5*, 3.

[24]. a) T. Asano, A. Sakai, S. Ouchi, M. Sakaida, A. Miyazaki, S. Hasegawa, *Adv. Mater.* **2018**, *30*, 1803075; b) X. Li, J. Liang, J. Luo, M. N. Banis, C. Wang, W. Li, S. Deng, C. Yu, F. Zhao, Y. Hu, T.-K. Sham, L. Zhang, S. Zhao, S. Lu, H. Huang, R. Li, K. R. Adaira, X. Sun, *Energy Environ. Sci.* **2019**, *12*, 2665-2671; c) K. Wang, Q. Ren, Z. Gu, C. Duan, J. Wang, F. Zhu, Y. Fu, J. Hao, J. Zhu, L. He, C.-W. Wang, Y. Lu, J. Ma, C. Ma, *Nat. Commun.* **2021**, *12*, 4410; d) L. Zhou, T.-T. Zuo, C. Y. Kwok, S. Y. Kim, A. Assoud, Q. Zhang, J. Janek, L. F. Nazar, *Nat. Energy* **2022**, *7*, 83-93; e) Y. Ishiguro, K. Ueno, S. Nishimura, G. Iida, Y. Igarashib, *Chem. Lett.* **2023**, *52*, 237-241; f) Y.-C. Yin, J.-T. Yang, J.-D. Luo, G.-X. Lu, Z. Huang, J.-P. Wang, P. Li, F. Li, Y.-C. Wu, T. Tian, Y.-F. Meng, H.-S. Mo, Y.-H. Song, J.-N. Yang, L.-Z. Feng, T. Ma, W. Wen, K. Gong, L.-J. Wang, H.-X. Ju, Y. Xiao, Z. Li, X. Tao, H.-B. Yao, *Nature* **2023**, *616*, 77-83.

[25]. X. Li, J. Liang, X. Yang, K. R. Adair, C. Wang, F. Zhao, X. Sun, *Energy Environ. Sci.* **2020**, *13*, 1429.

[26]. J. Liang, X. Li, K. R. Adair, X. Sun, *Acc. Chem. Res.* **2021**, *54*, 1023-1033.

[27]. C. Wang, J. Liang, J. T. Kim, X. Sun, *Sci. Adv.* **2022**, *8*, eadc9516.

[28]. a) F. Hao, Y. Liang, Y. Zhang, Z. Chen, J. Zhang, Q. Ai, H. Guo, Z. Fan, J. Lou, Y. Yao, *ACS Energy Lett.* **2021**, *6*, 201-207; b) J. Zhang, Z. Chen, Q. Ai, T. Terlier, F. Hao, Y. Liang, H. Guo, J. Lou, Y. Yao, *Joule* **2021**, *5*, 1-15.

[29]. W. Jia, X. Zhang, L. Xin, A. Luedtke, D. Zheng, H. Huang, T. Lambert, D. Qu, *Energy Storage Mater.* **2022**, *45*, 680-686.

[30]. X. Zhou, Y. Zhang, M. Shen, Z. Fang, T. Kong, W. Feng, Y. Xie, F. Wang, B. Hu, Y. Wang, *Adv. Energy Mater.* **2022**, 2103932.

[31]. W. Ji, X. Zhang, H. Qu, L. Xin, A. T. Luedtke, H. Huang, T. H. Lambert, D. Qu, *Nano Energy* **2022**, *96*, 107130.

[32]. F. Song, Z. Wang, G. Sun, T. Ma, D. Wu, L. Chen, H. Li, F. Wu, *eTransportation* **2023**, *18*, 100261.

[33]. F. Song, Z. Wang, T. Ma, L. Chen, H. Li, F. Wu, *Nano Energy* **2023**, *117*, 108893.

[34]. L. Oyster, H. Adkins, *J. Am. Chem. Soc.* **1921**, *43*, 208-210.

[35]. A. P. Hitchcock, Analysis of X-ray Images and Spectra (aXis2000): a toolkit for the analysis of X-ray.

[36]. K. Momma, F. Izumi, *J. Appl. Crystallogr.* **2011**, *44*, 1272-1276.

[37]. S. Gottis, A.-L. Barrès, F. Dolhem, P. Poizot, *ACS Appl. Mater. Interfaces* **2014**, *6*, 10870-10876.

[38]. a) W. Tao, H. Zhang, T. Jia, S. Luo, Q. Hou, Y. Wang, G. Shi, B. Xu, *J. Electrochem. Soc.* **2018**, *165*, A1574; b) X. Guo, Y. Zhang, H. Chen, C. Cui, Z. Li, Y. Du, B. Wang, H. Yang, *Int. J. Electrochem. Sci.* **2020**, *15*, 7774-7787.

[39]. a) S. Boulineau, M. Courty, J.-M. Tarascon, V. Viallet, *Solid State Ionics* **2012**, *221*, 1-5; b) C. Yu, F. Zhao, J. Luo, L. Zhang, X. Sun, *Nano Energy* **2021**, *83*, 105858.

[40]. K. W. Nam, H. Kim, Y. Beldjoudi, T.-W. Kwon, D. J. Kim, J. F. Stoddart, *J. Am. Chem. Soc.* **2020**, *142*, 2541-2548.

[41]. a) H.-D. Lim, H.-K. Lim, X. Xing, B.-S. Lee, H. Liu, C. Coaty, H. Kim, P. Liu, *Adv. Mater. Interfaces* **2018**, *5*, 1701328; b) J. Su, M. Pasta, Z. Ning, X. Gao, P. G. Bruce, C. R. M. Grovenor, *Energy Environ. Sci.* **2022**, *15*, 3805.

[42]. B. Ravel, M. Newville, *J. Synchrotron Rad.* **2005**, *12*, 537-541.

[43]. a) R. J. Hopkins, A. V. Tivanski, B. D. Marten, M. K. Gillesa, *J. Aerosol Sci.* **2007**, *38*, 573-591; b) V. Zelenay, R. Mooser, T. Tritscher, A. Křepelová, M. F. Heringa, R. Chirico, A. S. H. Prévôt, E.Weingartner, U. Baltensperger, J. Dommen, B.Watts, J. Raabe, T. Huthwelker, M. Ammann, *Atmos. Chem. Phys.* **2011**, *11*, 11777-11791; c) Z. Shadike, H.-S. Lee, C. Tian, K. Sun, L. Song, E. Hu, I. Waluyo, A. Hunt, S. Ghose, Y. Hu, J. Zhou, J. Wang, P. Northrup, S.-M. Bak, X.-Q. Yang, *Adv. Energy Mater.* **2019**, *9*, 1900705; d) G.-F. Han, F. Li, W. Zou, M. Karamad, J.-P. Jeon, S.-W. Kim, S.-J. Kim, Y. Bu, Z. Fu, Y. Lu, S. Siahrostami, J.-B. Baek, *Nat. Commun.* **2020**, *11*, 2209.

[44]. a) " XAFS spectrum of Zirconium chloride Anhydrous", can be found under https://doi.org/10.48505/nims.2965; b) J.J. Rehr, A.L. Ankudinov *Coord. Chem. Rev.* **2005**, *249*, 131-140.

[45]. a) H. Funke, A. C. Scheinost, M. Chukalina, *Phys. Rev. B* **2005**, *71*, 094110; b) H. Funke, M. Chukalina, A. C. Scheinost, *J. Synchrotron Rad.* **2007**, *14*, 426−432.

[46]. A. Jouhara, N. Dupré, A.-C. Gaillot, D. Guyomard, F. Dolhem, P. Poizot, *Nat. Commun.* **2018**, *9*, 4401.

[47]. P. W. Hart, J. T. Sommerfeld, *Cost Eng.* **1997**, *39*, 31-35.

[48]. a) L. Oyster, H. Adkins, *J. Am. Chem. Soc.* **1921**, *43*, 208-210; b) Liang, P. Zhang, J. Chen, *Chem. Sci.* **2013**, *4*, 1330; c) S. Wang, E. K. Todd, M. Birau, J. Zhang, X. Wan, Z. Y. Wang, *Chem. Mater.* **2005**, *17*, 6388-6394; d) Z. Song, H. Zhan, Y. Zhou, *Chem. Commun.* **2009**, 448-450; e) Z. Song, H. Zhan, Y. Zhou, *Angew. Chem. Int. Ed.* **2010**, *49*, 8444-8448; f) S. Wang, L. Wang, K. Zhang, Z. Zhu, Z. Tao, J. Chen, *Nano Lett.* **2013**, *13*, 4404-4409; g) D. S. Acker, W. R. Hertler, *J. Am. Chem. Soc.* **1962**, *84*, 3370-3374.

[49]. F. Han, J. Yue, X. Fan, T. Gao, C. Luo, Z. Ma, L. Suo, C. Wang, *Nano Lett.* **2016**, *16*, 4521-4527.

[50]. T. H. Wan, M. Saccoccio, C. Chen, F. Ciucci, *Electrochim. Acta* **2015**, *184*, 483-499.

[51]. a) Y. Lu, C.-Z. Zhao, J.-Q. Huang, Q. Zhang, *Joule* **2022**, *6*, 1172-1198; b) X. Li, J. Liang, J. T. Kim, J. Fu, H. Duan, N. Chen, R. Li, S. Zhao, J. Wang, H. Huang, X. Sun, *Adv. Mater.* **2022**, *34*, 2200856.

10.1002/anie.202403331

WILEY VCH

COMMUNICATION

Entry for the Table of Contents

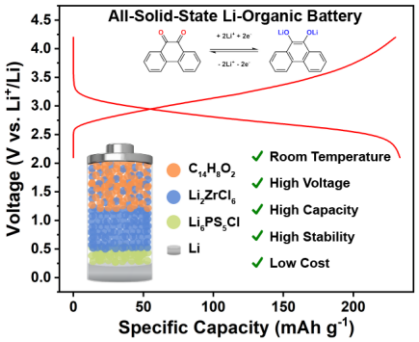

We design an all-solid-state lithium battery based on a cost-effective organic cathode material phenanthrenequinone (PQ) and a halide solid electrolyte Li_2ZrCl_6. The PQ cathode achieved a high specific capacity of 248 mAh g^{-1} (96% of the theoretical capacity), a high working voltage of 2.74 V (vs. Li^+/Li), and a good capacity retention of 95% after 100 cycles at room temperature (25 °C).